

# **APPLICATION OF CORE ANALYSIS TECHNIQUES FOR TIGHT ROCKS FOR THE INVESTIGATION OF BOREHOLE CEMENT**

Marisa B. Rydzy, James Heathman, Chad Broussard, Jorge Patino,  
Nours Elmetni, Aaron Dhaemers, and Matthias Appel  
Shell International Exploration and Production, Houston, TX

*This paper was prepared for presentation at the International Symposium of the Society of Core Analysts held in Vienna, Austria, 27 August – 1 September 2017*

## **ABSTRACT**

In this study, we performed water and gas permeability measurements on borehole cement using core analysis techniques that had previously been applied to nano-porous rocks, such as shale and tight sand. A series of plug-sized samples produced from five different cement mixtures were subjected to water and gas permeability measurements, nuclear magnetic resonance (NMR) spectroscopy, mercury injection capillary pressure (MICP) tests, and micro x-ray computed tomography (MXCT) scans. The water permeability of all cement plugs fell in the low nano-Darcy range. The difference in permeability among cement types was small but consistent and appeared to be primarily a function average pore size (calculated as weighted average) as indicated by MICP (and NMR). Results from time-dependent water permeability and NMR measurements showed a decrease in permeability and pore size as cement continued to cure. MXCT images of the tested plugs revealed the presence of bubbles within the cement. With the help of basic digital rocks analysis technology, we were able to quantify the size and amount of the bubbles and calculate a bubble size distribution for each imaged sample. Overall, the bubbles did not contribute significantly to the cement porosity (less than 1 porosity unit). Other than introducing a certain degree of heterogeneity, the isolated void spaces appeared not to affect the fluid flow. Gas permeabilities were measured after the samples had been dried. The resulting permeability values were higher than the ones measured with water by orders of magnitude which was likely due to drying-induced fractures and gas slippage.

## **INTRODUCTION**

The main purpose of borehole cement is to provide a hydraulic seal between casing and formation (Nelson, 1990) over the lifetime of a well. The permeability of cement not only characterizes its effectiveness as a sealant but also provides a measure of durability

(Manmohan and Metha, 1981; Bathia and Mindness, 1989). The pore structure of cement depends on variety factors, including the composition of the cement mixture (class, water-cement ratio, additives), as well as setting time and temperature (e.g. Goto and Roy, 1981; Talabani and Hareland, 1995; Atahan et al., 2009). Cement represents physically and chemically complex nano-porous system. Portland cement represents the most common type of hydraulic cement and is primarily composed of finely powdered tricalcium silicate, dicalcium silicate, tricalcium aluminate, and tricalcium aluminoferrite, as well as small amounts of gypsum (Michaux et al., 1990). Depending on the fraction of each of these compounds Portland cement is divided into 8 groups (Classes A-H; Nelson, 1983). When the cement components are mixed with water, a chemical reaction between compounds and water occurs (a.k.a. hydration), whereby an unstable, supersaturated solution is formed from which new solids precipitate and grow into the water-filled pore space. As cement hardens (sets, cures, or ages), its compressive strength increases while porosity and permeability decline (e.g. Powers, 1956; Michaux et al. 1990).

A number of studies have been dedicated to the investigation of Portland cement permeability. The very first cement permeability results that were published, had been obtained from gas flow experiments on dried cement plugs (Coleman and Corrigan, 1940). Morgan and Dumbauld (1952), questioned the approach as drying of set cement was (and still is) believed to alter its physical and chemical properties. They recognized that permeability measurements on cement needed to be conducted with water, which became the standard approach in the following years. Subsequent publications presented results from water permeability measurements of cement as functions of cement-water ratio, curing time and temperature, cement fineness, pore size distribution, and content of a variety of additives (e.g. Manmohan and Metha, 1981; Nyame and Illston, 1981; Banthia and Mindness, 1989; Talabani and Hareland, 1995; Ai et al., 2001; Vichit-Vadakan and Scherer, 2002, 2003; Ye, 2005, and many more). With the advance of computational capabilities in recent years, pore-network models and simulations have become the focus of cement permeability studies (Zalzale et al., 2010; Hu and Stroeven, 2011; Wong et al., 2012). Interestingly, the simulation results best corresponded with gas permeabilities measured in dried cement plugs, which may have prompted a resurgence of this measurement approach as the most recent cement permeability measurements have been conducted with gas (Wong et al., 2009; Zhang et al., 2014; LeMinous et al., 2017). Overall, published cement permeability results vary widely and range over several orders of magnitude from nd to md range. Aside, from the effect of compositional differences and curing time/conditions, a number of other reasons have been proposed to explain the wide data spread, including delayed hydration, fines migration, or variation in water saturation (Zalzale et al. 2010). In addition, some inconsistency can surely be attributed to the differences in measurement procedures and data quality.

In this study, we tested a series of cement plugs formed from a number of different cement mixtures. The main focus on the study were on water (and gas) permeability measurements that were conducted with experimental setups that had previously been used to measure ultra-low permeabilities in nano-porous rocks, such as shales. The objective of the study at hand was to compare permeabilities of different cement types and to observe the time-dependency of their permeability response. Micro X-ray computed tomography images of the plugs, NMR T2 spectra, and pore-size distribution curves from mercury injection capillary pressure tests were also acquired to aid in the interpretation of the permeability data.

## SAMPLES AND EXPERIMENTAL PROCEDURES

We tested plugs that had been prepared from 5 different Portland cement mixtures (API classes H, A, or G with a variety of different additives, [Table 1](#)) according to API RP 10B-2 specifications. The cement slurries had been poured into 2.54-cm diameter cylindrical molds and allowed to cure for 1 week. The resulting cement plugs were cut/trimmed to a length of about 2.54 cm and weighed. The amount of free water in the cement plugs was determined based on T2 measurements with a 2 MHz nuclear magnetic resonance (NMR) spectrometer. [Table 1](#) provides an overview of the different cement types tested as well as a summary of cement plug properties, such as the average plug density, volume fraction of unbound water (NMR-Phi), and the logarithmic average of the relaxation time (Log Mean T2). The latter is loosely related to the average pore size. All values listed in [Table 1](#) represent an average of results from tests on at least 8 cement plugs. Water permeability measurements were performed on 2-4 plugs per cement type.

**Table 1:** Overview of cement samples and their average properties (W/C mass ratio of water and cement)

Cement	Description	W/C	Strength	$\rho$ , g/cc	$\phi_{\text{NMR}}$ , %	Mean T2
C-1	Class H	0.39	5150 psi	2.00±0.04	0.328±0.001	0.481±0.021
C-3	Class H + KCl + dead-burnt manganese oxide	0.36	5179 psi	2.09±0.04	0.358±0.011	0.343±0.008
C-4	Class H + dead-burnt manganese oxide + SBR latex	0.23	5592 psi	2.08±0.06	0.272±0.004	0.282±0.005
C-5	Class A + KCl + silica flour	0.59	3271 psi	1.92±0.07	0.472±0.017	0.516±0.009
C-7	Class G + KCl	0.46	4399 psi	1.98±0.01	0.340±0.008	0.389±0.006

The permeability measurements were conducted using Hassler-type flow cell (Hassler, 1944). The liquid permeameter systems had been designed, constructed, and previously employed for permeability measurements in nano-porous rocks, such as shales (Rydzy et al. 2016). The water permeabilities were measured with DI-water under an effective stress of 4.5 MPa (650 psi) using the steady-state technique. Inlet and outlet pore pressure were set to 6.9 MPa (1000 psi) and 0.7 MPa (100 psi), respectively, resulting in a pressure differential of 6.2 MPa (900 psi) across the plug. The injected water volume was recorded as function of time. From the resulting flow rate, the pressure differential, sample length

and diameter, as well as the water viscosity (1 cP at 30°C), the permeability was calculated using Darcy's Law (e.g. Peters 2012).

In addition to the water permeability testing, we performed gas permeability measurements on dried cement plugs. (The experimental setup is described in Rydzy et al., 2016). The dried cement plugs were subjected to pulse-decay tests under varying effective stresses (from 3.4 to 24.1 MPa or 500-3500 psi in increments of 3.4 MPa or 500 psi). Following the permeability measurements, we acquired micro X-ray CT (MXCT) images of the cement plugs and generated bubble size distribution curves based on the MXCT images using the 3D Object Counter Function in the open source image analysis software IMAGEJ (<https://imagej.nih.gov/ij/>). The process is shown in **Figure 1**. We also acquired mercury injection capillary pressure (MICP) curves of crushed dried cement particles (particle size between 0.5 and 2.38 mm) from which we calculated weighted pore-throat size averages (**Figure 2**). The MICP measurements were conducted after the samples had been exposed to atmosphere for over 2-4 months. Directly prior to the MICP measurements the plugs had been dried under vacuum at 80°F for about 2 days.

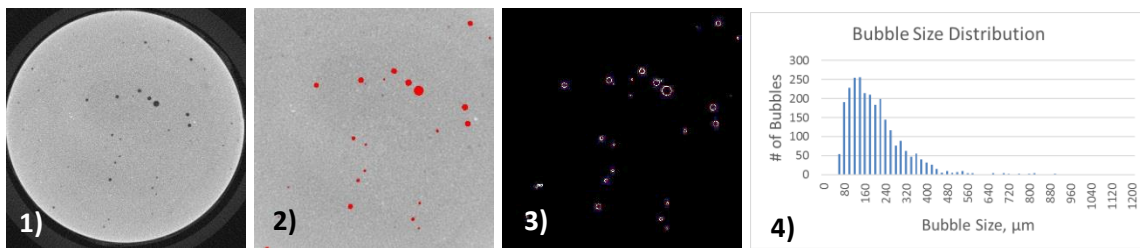


**Figure 1:** Process of determining a bubble size distribution: the original image (1) was loaded into IMAGEJ and cut into an 800x800x800 pixel3 image volume. A 3D mean filter was applied before the image was segmented (2). The 3D Object Counter Plugin was then run on the segmented image (3). The program data output could then be used to generate a bubble size distribution for the respective plug (4).

## RESULTS AND DISCUSSION

After a fast initial hydration reaction, unreacted cement compounds end up being enclosed by a layer of impermeable precipitate. The hydration reaction then becomes diffusion controlled and slows down significantly. Hydration continues with decreasing speed for as long as water and anhydrous compounds are present. This process can take an infinite amount of time. According to Michaux et al. (1990), complete hydration is never attained. As cement sets, its porosity, pore sizes, and permeability continue to decrease. The decrease in these physical properties over time could be observed in results of the water permeability measurements (**Figure 3**).

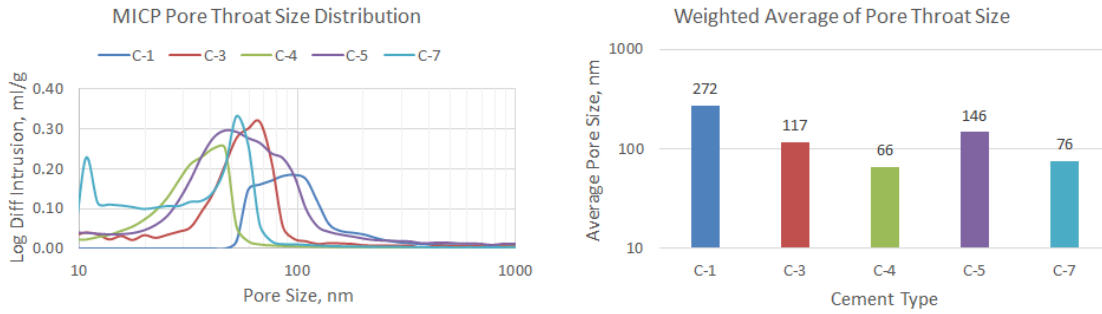


**Figure 2:** Mercury injection capillary pressure (MICP) pore-throat size distributions obtained for dried cement particles (particle size: 0.5-2.38 mm, left) and the weighted pore throat size average calculated from the MICP data (right)

The water permeability of all samples, except the Cement 4 (C-4) plugs, had been measured over the course of 11 days (Figure 3). With the exception of Cement 1 (C-1) all cements had been allowed to set for 10 to 13 days before they were subjected to the water permeability tests. Overall, the water permeability of all samples fell in the low nano-Darcy range with values between 0.5 and 10 nd. The permeability of C-1 plugs was higher than the permeability of all other cements despite the extended setting period. Backward extrapolation of its permeability-time trend approximates a permeability of around 200 nd for the 10<sup>th</sup> day of curing. Figure 3 also shows the water permeability of all tested cement plugs averaged over all 11 test days. Even though the difference between permeabilities for different cement types was rather small, the results were consistent among plugs from the same cement batch.

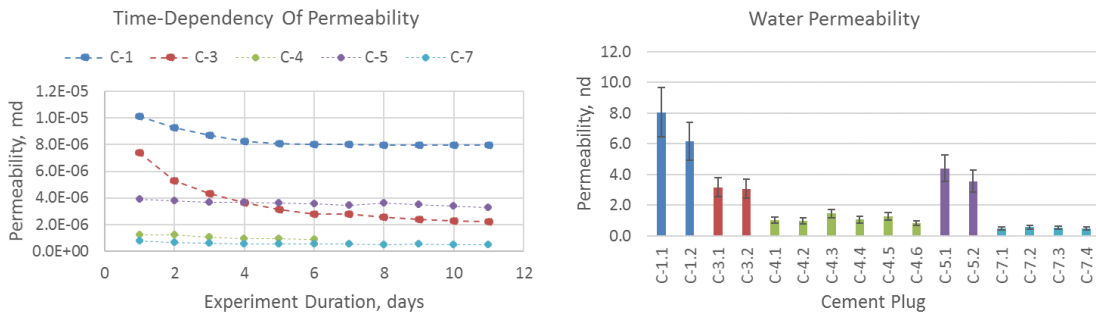


**Figure 3:** Decrease in water permeability over time (for clarity, only results for 1 plug per batch are shown) and water permeability of all plugs average over all 11 test days

Figure 4 shows the water permeability as a function of NMR-derived porosity, the pore size proxy Log Mean T2, and the MICP-derived weighted average of the pore-throat size distribution. Due to the time-sensitive nature of the results, the permeability values plotted against the NMR data were the ones recorded on the first day of testing as the NMR measurements were performed prior to the water permeability measurements. The MICP

measurements were performed after the permeability was measured. Consequently, the permeability values recorded on the last day of testing were plotted against the weighted average of the pore-throat size distribution. Early discussions regarding fluid flow in cement revolved around the question whether it was porosity, pore size distribution, or pore threshold diameter that determined the cement permeability (Goto and Roy, 1981). The results shown in **Figure 4** clearly indicate that porosity and pore size have little effect on the water permeability overall. A clear correlation, however, was found between the weighted average of the pore-throat diameter distribution (for pore throats smaller than 1000 nm) and the cement permeability measured with water.

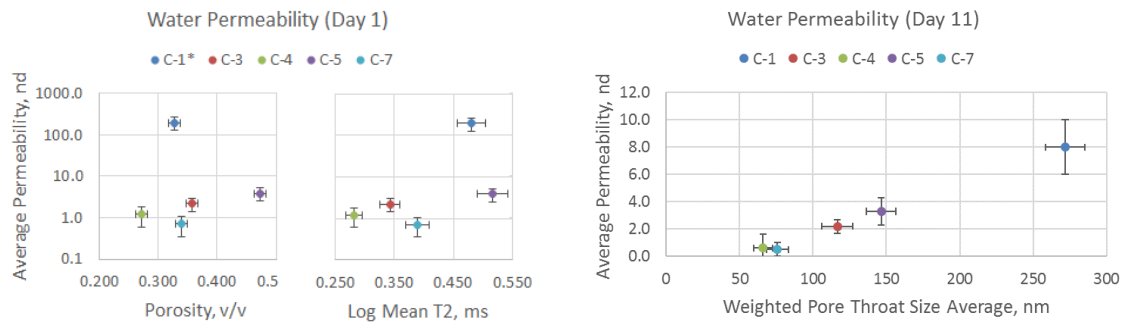
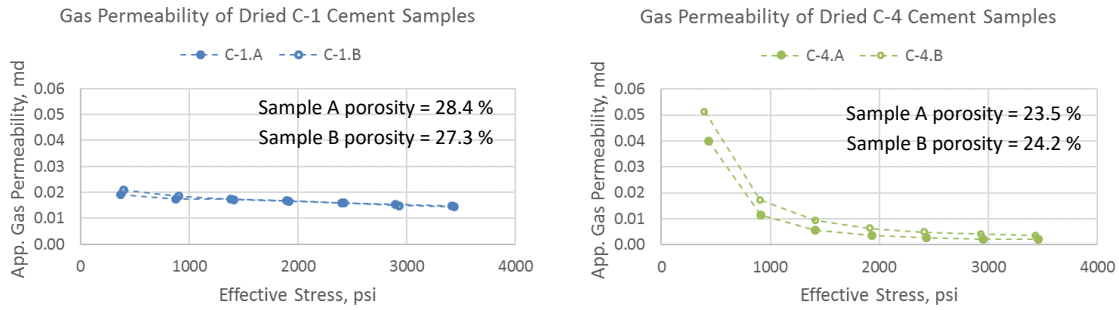


**Figure 4:** Average water permeability depicted as function of porosity, logarithmic average of the relative pore-size proxy T2, and weighted average of the pore-throat diameter distribution.

After the water-permeability measurements, we dried 4 additional plugs from 2 different cement types (C-1 and C-4), and subsequently performed unstressed helium porosimetry and stressed gas permeability measurements on them. The results are shown in **Figure 5**. The gas permeability values are significantly higher than the corresponding water permeability measurements by several orders of magnitude. At 500 psi effective stress, we obtained permeabilities of  $2 \cdot 10^5$  nd and  $4.5 \cdot 10^5$  nd for C-1 and C-4 plugs, respectively. These results were typical for gas permeabilities measured in dried Portland cement samples which have been reported as  $10^{-17}$ - $10^{-19}$  m<sup>2</sup> (Wong et al. 2009; Zhang and Talman, 2014; Le-Minous et al. 2017), which corresponds to  $10^5$ - $10^7$  nd. One reason for the elevated permeability values can be attributed to gas slippage (Klinkenberg, 1941), as the measurements were conducted at an average pore pressure of only 0.7 MPa (100 psi). Gas slippage alone was unlikely to account for the elevated permeability values. Many authors of previous studies suggested that micro-cracks were created by the drying process (e.g. Morgan and Dumbauld, 1952; Talabani and Hareland, 1995; Wong et al. 2009). If micro-cracks were responsible for the increased permeability, it could be assumed, based on the stress-permeability trend, that the plugs of the C-4 cement contained more cracks than the plugs of C1-cement. The C-4 plugs exhibit a much stronger stress-dependency than the C1-plugs (**Figure 5**), despite its compressional strength being higher (**Table 1**).



**Figures 5:** Results of gas permeability measurements on dried cement plugs

Following the permeability measurements, we acquired MXCT scans of the cement plugs to investigate the degree of heterogeneity in the samples. The MXCT images (**Figure 6**) show that isolated spherical void spaces (bubbles) are randomly spread throughout the samples. Quantitative analysis confirmed that number of bubbles, the volume occupied by them, and their size distribution varied between cement types. For example, C-4 plugs exhibited a large number ( $>10,000$ ) of relatively small bubbles (average bubble size = 123  $\mu\text{m}$ ), while C-5 and C-7 plugs contained less bubbles (in the 1000s) of much larger size (average bubble size around 190  $\mu\text{m}$ ). Cements C-1 and C-3 contained the least amount of bubbles (in the 10s, with average bubble size of around 180  $\mu\text{m}$ ). The volume occupied by bubbles on average only contributed 0.2 to a maximum of 1% (1 porosity unit) to the overall porosity of the cement. As the permeability was primarily a function of the pore throat size distribution and bubbles occurred mostly isolated, we concluded that the effect of the presence of bubbles could be assumed negligible.

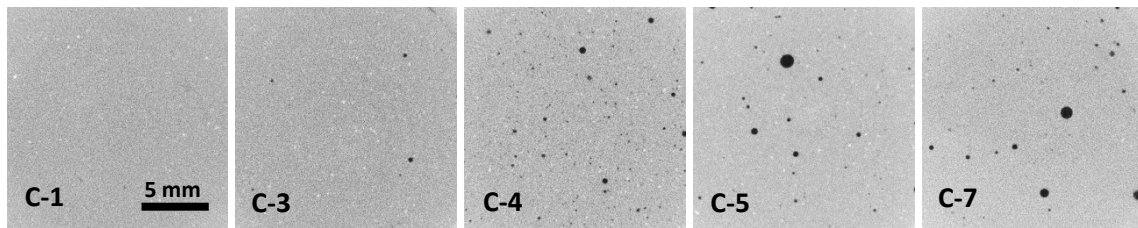


**Figure 6:** MXCT images (16 mm x 16 mm, pixel length = 20  $\mu\text{m}$ ) of cement plugs.

## CONCLUSIONS

In this paper, we presented observations and results from core analysis measurements on different types of borehole cement. It was shown that water and gas permeability measurement techniques that had previously been developed for nano-porous rocks, such as shale and tight sand, could be successfully applied to test the nano-porous cement samples. NMR was also shown to be a useful tool for the characterization of the cement plugs as it provided porosity data and some information regarding the relative pore size of the cements. Using MXCT and basic digital rocks analysis techniques we quantitatively

analyzed the larger void spaces (bubbles) in the cement plugs. Results for gas and water permeability, porosities, Log Mean T2, and pore-throat size distribution were consistent among cement plugs stemming from the same batch. It was shown that water permeability was primarily a function of the pore throat size distribution and the curing time. Log Mean T2, and the presence of bubbles in the cement plugs appeared to have little effect on the outcome of the permeability results. As for the way forward:

- Time-dependent NMR measurements could provide additional insight into the effect of the setting process on the pore structure of cement. Note that in between tests the cement plugs would have to be stored in water at a constant temperature to prevent partial drying of the sample and to allow for consistent cement setting kinetics.
- As the bubbles introduce a certain degree of heterogeneity, their presence could theoretically be responsible for the small variation in permeability observed among the plugs of the same cement type. To tests this hypothesis a relatively large number of samples (e.g.  $\geq 4$ ) would have to be tested and imaged to be statistically representative.
- The gas permeability behavior of dried samples under stress may provide insight on how much the cement may have fractured during the drying process. This could be confirmed through higher-resolution imaging of the dried samples.

## REFERENCES

- Ai, H., Young, J. F., & Scherer, G. W. (2001). Thermal expansion kinetics: method to measure permeability of cementitious materials: II, application to hardened cement pastes. *Journal of the American Ceramic Society*, 84(2), 385-91.
- Atahan, H. N., Oktar, O. N., & Taşdemir, M. A. (2009). Effects of water–cement ratio and curing time on the critical pore width of hardened cement paste. *Construction and Building Materials*, 23(3), 1196-1200.
- Banthia, N., & Mindess, S. (1989). Water permeability of cement paste. *Cement and Concrete Research*, 19(5), 727-736.
- Coleman, J. R., & Corrigan, G. L. (1941). Fineness and water-cement ratio in relation to volume and permeability of cement. *Transactions of the AIME*, 142(01), 205-215.
- Dewaele, P. J., Reardon, E. J., & Dayal, R. (1991). Permeability and porosity changes associated with cement grout carbonation. *Cement and concrete research*, 21(4), 441-454.
- Goto, S., & Roy, D. M. (1981). Diffusion of ions through hardened cement pastes. *Cement and Concrete Research*, 11(5-6), 751-757.
- Hearn, N., Hooton, R. D., & Mills, R. H. (1994). Pore structure and permeability. In *Significance of tests and properties of Concrete and Concrete-Making Materials*. ASTM International.

- Hassler, G.L., 1944. Method and apparatus for permeability measurements. US2345935 A.
- Hu, J. and Stroeven, P., 2011. Application of image analysis to assessing critical pore size for permeability prediction of cement paste. *Image Analysis & Stereology*, 22(2), pp.97-103.
- Klinkenberg, L. (1941). The permeability of porous media to liquids and gases. *Drilling and Production Practice*. American Petroleum Institute.
- LeMinous, J.C., Mutti, D., Bouvet, A., Massie, I., Xiao, E., & Schnell, E. (2017), Permeability Study of API Class G and B Cements considering Seawater and WBM Contamination, SPE/IADC-184613-MS
- Li, S., & Roy, D. M. (1986). Investigation of relations between porosity, pore structure, and C1– diffusion of fly ash and blended cement pastes. *Cement and Concrete Research*, 16(5), 749-759.
- Luping, T., & Nilsson, L. O. (1992). A study of the quantitative relationship between permeability and pore size distribution of hardened cement pastes. *Cement and concrete research*, 22(4), 541-550.
- Manmohan, D., & Mehta, P. K. (1981). Influence of pozzolanic, slag, and chemical admixtures on pore size distribution and permeability of hardened cement pastes. *Cement, Concrete and Aggregates*, 3(1), 63-67.
- Michaux, M., Nelson, E. B., & Vidick, B. (1990). 2 Chemistry and Characterization of Portland Cement. *Developments in Petroleum Science*, 28, 2-1.
- Morgan, B. E., & Dumbauld, G. K. (1952). Measurement of the Permeability of Set Cement. *Journal of Petroleum Technology*, 4(06), 16-10.
- Nelson, E. B. (Ed.). (1990). *Well cementing* (Vol. 28). Newnes.
- Nyame, B. K., & Illston, J. M. (1981). Relationships between permeability and pore structure of hardened cement paste. *Magazine of Concrete Research*, 33(116), 139-146.
- Peters, E. J. (2012). *Advanced Petrophysics: Volume 1: Geology, Porosity, Absolute Permeability, Heterogeneity and Geostatistics*. Live Oak Book Co, Austin, Texas.
- Powers, T. C. (1958). Structure and physical properties of hardened Portland cement paste. *Journal of the American Ceramic Society*, 41(1), 1-6. WILEY
- Vichit-Vadakan, W., & Scherer, G. W. (2002). Measuring Permeability of Rigid Materials by a Beam-Bending Method: III, Cement Paste. *Journal of the American Ceramic Society*, 85(6), 1537-1544.
- Vichit-Vadakan, W., & Scherer, G. W. (2003). Measuring permeability and stress relaxation of young cement paste by beam bending. *Cement and Concrete Research*, 33(12), 1925-1932.
- Wong, H. S., Zobel, M., Buenfeld, N. R., & Zimmerman, R. W. (2009). Influence of the interfacial transition zone and microcracking on the diffusivity, permeability and sorptivity of cement-based materials after drying. *Mag. Concr. Res*, 61(8), 571-589.

Wong, H. S., Zimmerman, R. W., & Buenfeld, N. R. (2012). Estimating the permeability of cement pastes and mortars using image analysis and effective medium theory. *Cement and Concrete Research*, 42(2), 476-483.

Ye, G. (2005). Percolation of capillary pores in hardening cement pastes. *Cement and concrete research*, 35(1), 167-176.

Zalzale, M., McDonald, P. J., & Scrivener, K. L. (2013). A 3D lattice Boltzmann effective media study: understanding the role of CSH and water saturation on the permeability of cement paste. *Modelling and Simulation in Materials Science and Engineering*, 21(8), 085016.